small bristles Is Required for the Morphogenesis of Multiple Tissues During Drosophila Development

Christopher A. Korey,* Gavin Wilkie,† Ilan Davis† and David Van Vactor*

**Department of Cell Biology, The Program in Neuroscience and The Dana Farber Cancer Institute/Harvard Cancer Center, Harvard Medical School, Boston, Massachusetts 02115 and †Wellcome Trust Centre for Cell Biology, ICMB, University of Edinburgh, Edinburgh EH9 3JR, Scotland*

Manuscript received July 12, 2001
Accepted for publication October 1, 2001

ABSTRACT

We found that mutations in *small bristles (sbr)* affect several tissues during the development of the fruit fly. In *sbr* embryos, neurons have defects in pathfinding and the body wall muscles have defective morphology. As adults, *sbr* flies have smaller and thinner bristles with a reduced diameter, suggesting a defective cytoskeleton within. The phenotypes we observe are consistent with defects in cell morphogenesis. We identified DmNXF1, the Drosophila homolog of a mRNA export protein that has been characterized in human (NXF1/TAP) and yeast (Mex67p) as the protein encoded by the *small bristles* locus. Given that a global decrease in mRNA export in these mutants is likely, the phenotypes we observe suggest that certain tissues are acutely sensitive to lower levels of cytoplasmic mRNA and the resultant decrease in protein synthesis during key stages of cellular morphogenesis.

THE development of a multicellular organism requires that cells undergo a complex and sometimes rapid morphogenesis to form the distinct tissues that are required for normal function. To accomplish this, genes are expressed and translated into the proteins that orchestrate the formation of each tissue type. The coordination of this process entails a complex communication between the extracellular milieu, the cytoplasm, and the nucleus. This results in the production of the signaling and structural proteins required for the formation and function of the resultant tissues and organs. While this process may be gradual in different cell types, certain cells undergo very rapid and complex morphogenesis such as the gametes, flight muscles, and sensory bristles of adult Drosophila. It has been postulated that such cells require higher levels of protein synthesis to accommodate their rapid rate of development (Lambertsson 1998). While high levels of protein synthesis put heavy demands on ribosomal function, rapid synthesis will also require the expeditious export of mRNA to supply the translation machinery. While the mechanisms of mRNA export are being rapidly elucidated in yeast and higher eukaryotes, the pathways underlying this phenomenon and their functions in metazoan development are still poorly understood.

One important step toward understanding RNA export in higher eukaryotes was the discovery of how retroviruses, particularly Mason-Pfizer monkey virus (MPMV), get their spliced and unspliced viral RNA into the cytoplasm of infected cells. In a normal cellular context, unspliced preRNAs are retained within the nucleus. Retroviruses require that their full-length unspliced RNA be exported from the nucleus to produce viral proteins and to be packaged into new viral particles. To accomplish this the MMPV viral RNA contains a constitutive transport element (CTE) that mediates efficient export of unspliced RNA out of the cell nucleus (Bray *et al.* 1994; Tabernero *et al.* 1996). Unlike the HIV retrovirus's Rev protein, the simple MPMV does not encode for an equivalent protein, suggesting that a cellular protein must provide this service. *T*ip *a*ssociating *p*rotein/*n*uclear e*x*port *f*actor 1 (TAP/NXF1) was identified as a protein that specifically binds the CTE and mediates efficient export of CTE-containing RNA out of the nucleus (Grüter *et al.* 1998). Further experiments in Xenopus oocytes showed that injecting saturating amounts of CTE RNA prevented the export of mRNA, implying that TAP/NXF1's true cellular role lies in mRNA export (Pasquinelli *et al.* 1997; Saavedra *et al.* 1997; Grüter *et al.* 1998).

Previous to the identification of human TAP (TAP/NXF1), work in *Saccharomyces cerevisiae* identified the yeast homolog, *mex67*, in a screen for genes required for the export of poly(A)$^+$ RNA (Segref *et al.* 1997). Mex67p localizes to the nuclear rim and was shown to bind and mediate the export of RNA polymerase II transcripts (Segref *et al.* 1997; Hurt *et al.* 2000). Subsequent work in both systems has clearly identified four functional domains within the TAP/NXF1 protein. At the N terminus, TAP/NXF1 has a noncanonical ribonucleoprotein (RNP)-type RNA binding domain and a leucine-rich repeat region (LRR; Liker *et al.* 2000).

Corresponding author: David Van Vactor, Department of Cell Biology, Harvard Medical School, 240 Longwood Ave.-LHRRB Rm. 401A, Boston, MA 02115. E-mail: davie@hms.harvard.edu

Together these domains mediate the specific binding of TAP/NXF1 to the viral CTE (Liker *et al.* 2000), while only the LRR is required for the export of mRNA in TAP/NXF1 (Braun *et al.* 2001). The next domain is an NTF-2-like domain that serves as the binding site for its partner protein p-15 (human, Herold *et al.* 2000; Suyama *et al.* 2000)/ Mtr2p (*S. cerevisiae*, Santos-Rosa *et al.* 1998; Sträßer *et al.* 2000). Efficient export of mRNA into the cytoplasm requires the formation of Mex67p-Mtr2p and TAP/NXF1-p15 complexes (Sträßer *et al.* 2000; Braun *et al.* 2001). Importantly, TAP/NXF1-p15 can substitute for Mex67p-Mtr2p in yeast cells, indicating a conserved mRNA export function for the complex (Katahira *et al.* 1999).

The C termini of TAP/NXF1 and Mex67p have been shown to bind to nucleoporins through a domain similar to a ubiquitin-associated (UBA) domain (Suyama *et al.* 2000). Studies have shown that the C terminus, which includes the UBA-like domain and part of the NTF2-like domain, is necessary and sufficient to localize TAP/NXF1 to the nuclear rim (Bear *et al.* 1999; Bachi *et al.* 2000; Herold *et al.* 2000). Finally, consistent with its role in the export of mature mRNAs out of the nucleus, several TAP/NXF1 binding proteins that associate with mRNA during and after splicing is completed have been identified, for example, Yra1p/REF (Sträßer and Hurt 2000; Stutz *et al.* 2000). Along with TAP/Mex67p's general affinity for mRNA, these proteins may also help recruit TAP/Mex67p to fully processed and spliced mRNA.

The recent identification of the *Caenorhabditis elegans* homolog, CeNXF1, showed that this protein is essential for viability of embryos and adults (Tan *et al.* 2000). However, the consequence of CeNXF1 loss-of-function on cellular development was not examined. Here we describe the developmental characterization of *small bristles (sbr*). We identified a new allele of *sbr* in an axon guidance screen and report that *small bristles* is required for a diverse set of morphogenetic events including motor-axon pathfinding, embryonic muscle development, and normal adult bristle formation. Our subsequent cloning of *sbr* identified DmNXF1, the Drosophila homolog of TAP/NXF1, as the protein encoded by this locus. Preliminary studies confirm that this gene is required for efficient export of mRNAs out of Drosophila nuclei (G. Wilkie, C. A. Korey, D. Van Vactor and I. Davis, unpublished observations). In light of our findings and this protein's role in mRNA export, we suggest that the developmental phenotypes observed indicate that cells undergoing rapid morphogenesis have an acute sensitivity to the loss of cytoplasmic mRNA and the resultant decrease in protein synthesis.

MATERIALS AND METHODS

Histology: Embryos were processed as described (Van Vactor and Kopczynski 1999). The following antibodies were used: mAb FMM5 (anti-myosin heavy chain, 1:10; Kiehart and Feghali 1986), mAb 2B8 (anti-Even-skipped, 1:50; Patel *et al.* 1994), mAb 1D4 (anti-fasciclin II, 1:4; Van Vactor *et al.* 1993), and mAb anti-β-galactosidase (1:500; Sigma, St. Louis; Van Vactor and Kopczynski 1999). mAb anti-β-galactosidase was used to recognize the β-galactosidase protein being produced by a transgene on the Fm7cβ balancer chromosome (β signifies the transgene). This transgene allowed for the identification of male embryos that would be hemizygous for *small bristles*.

Scanning electron microscopy: Newly eclosed female adults of the specified genotypes were collected and aged for several days in a yeast-free food vial. These flies were then taken through a series of ethanol dehydration steps. They were first placed in 25% ethanol and after a 12-hr incubation time they were moved to 50% ethanol. This process continued, moving through the following dilutions: 50, 75, 95, and 2× 100% ethanol. They were left in 100% ethanol and taken to the Northeastern Electron Microscopy facility to be critical point dried and sputter coated for scanning electron microscopy (SEM).

Germline clone: The *y w sbr^{mgln}* chromosome was recombined onto a FRT101 chromosome to incorporate the FRT sites to be used for the germline clone. Females of the genotype *y w sbr^{mgln}* FRT101/FM7cβ were then mated to males of the genotype *ovo^{D1}* FRT101/Y; hsFLP. When wandering third instar larvae were observed the vials were heat-shocked at 37° for 2 hr and then again for 2 hr, 24 hr later. A subset of these vials was not heat-shocked and served as the non-heat-shock control. As a wild-type germline clone control we crossed the original *y w* FRT101 females to males of the genotype *ovo^{D1}* FRT101/Y; hsFLP and followed the same procedure as outlined for the *sbr^{mgln}* chromosome. When the adults from the heat-shocked and non-heat-shocked vials eclosed, females of the genotype *y w sbr^{mgln}* FRT101/ *ovo^{D1}* FRT101 (experimental) or *y w* FRT101/ *ovo^{D1}* FRT101 (wild-type control) were collected. Four crosses were set up to determine the result of the germline clone induction: *y w sbr^{mgln}* FRT101/ *ovo^{D1}* FRT101 × FM7cβ/Y (one for heat shock and one for non-heat-shock control) and *y w* FRT101/ *ovo^{D1}* FRT101 × FM7cβ/Y (one for wild-type heat-shock control and one for wild-type non-heat-shock control).

Fly stock maintenance: All fly strains were raised at 25°.

Genetic mapping: Three multiply marked X chromosomes were used to genetically map the *sbr^{mgln}* lesion in relation to the chosen visual markers. The genotypes of the chromosomes were as follows: *sc ec cv ct g*, *y m wy sd os*, and *y cv v f car* (abbreviations according to Lindsley and Zimm 1992). On the basis of the recombinant classes and numbers of each class obtained, the *sbr^{mgln}* lesion's location was determined in relation to the experimental markers. On the basis of the results of the initial mapping, this analysis was done again with the *vermilion* eye marker alone. The high number of progeny counted for this analysis allowed us to calculate a map distance between *vermilion* and *sbr^{mgln}*.

The full deficiency kit for the X chromosome was obtained from the Bloomington Drosophila Stock Center. In addition, all chromosomal duplications that contained duplicated segments of the X chromosome were also obtained. These stocks were then independently crossed to the *sbr^{mgln}* line to obtain a duplication that rescued the lethality. Once we had identified such a duplication, *Dp(1;Y)v^{+}y^{+}*, we used rescued males (*yw mgln*/Y- *Dp(1;Y)v^{+}y^{+}*) to map *sbr^{mgln}* using the deficiency collection.

Deficiency breakpoint mapping: *Df(1)HC133:* Southern blots were done on genomic DNA preparations of three different genotypes: wild-type genomic DNA to view the normal digestion patterns; Df(1)HC133 to look for signs of a chromo-

somal breakpoint; and Df(1)v-L15, a deficiency that removes the entire region as a control for 50% DNA content. The PCR-amplified probe that identified the breakpoint, 929IJ (forward primer 5′ GAGGGGCAAACTTCATGTTAT 3′; reverse primer 5′ GCTTCAACAGCAGAAAAGAAC 3′), covered the 5′-most section of the *dIMP*. Analysis of the hybridization pattern showed a band shift indicative of a chromosomal lesion with four different restriction enzymes: *Hin*dIII, *Eco*RI, *Bam*HI, and *Bgl*II. The bandshifts predicted that the breakpoint resided in the ~1.3 kb between a *Bam*HI site and *Hin*dIII site in the 5′ untranslated region (UTR) of *dIMP*. Further Southern analysis with probes within the predicted deficiency region showed a 50% reduction in signal in flies heterozygous for the deficiency.

Df(1)vL4: We probed genomic blots with a PCR-amplified DNA fragment, 912QP (forward primer 5′ CGGATTGCACAG GAGATTCTGC 3′; reverse primer 5′ GGAAAACTCTGTTCA GCTCTG 3′), which contained the genomic DNA ~5 kb from the 3′ end of *sbr*. Analysis of this hybridization showed a band shift indicative of a chromosomal lesion with five different enzymes, *Hin*dIII, *Eco*RI, *Bam*HI, *Bgl*II, and *Sal*I. The band shifts predict that the breakpoint resides within a 2.5-kb *Eco*RI fragment. This implies that Df(1)v-L4 removes the *sbr* coding region. We confirmed this prediction by probing Southern blots with a genomic fragment that contained *sbr* coding sequence to show a 50% reduction in Df(1)v-L4/Fm7cβ signal as compared to wild type.

Df(1)vL3: Genomic Southern blots were probed with a DNA fragment from the K3.18.7 phage that contained the genomic DNA that included the 5′ end of *sbr*. Analysis of the hybridization pattern showed a band shift indicative of a chromosomal lesion with two different enzymes, *Sal*I and *Hin*dIII. The band shifts predict that the breakpoint resides within a 7.5-kb *Sal*I fragment. Further Southern analysis confirmed that the break was within the 4.7-kb *Hin*dIII-*Sal*I fragment that covers the 5′ end of *sbr*.

Restriction fragment length mapping: Restriction fragment length polymorphism (RFLP) mapping was performed as described by van der Bliek and Meyerowitz (1991). Twenty-three recombinant lines were obtained from the *vermilion-sbr^{mgln}* meiotic mapping cross. Each line had an independent recombination event between *vermilion* and the *sbr* locus. We obtained phage clones from the Zhimulev genomic walk that covered the region between *vermillion* and the putative location of the *sbr* locus (all clone names are stated as reported in Kozlova *et al.* 1994). These two reagents were used to determine the precise location of the mutation by RFLP analysis. The parent *vermilion* and *sbr^{mgln}* lines were cut with a battery of restriction enzymes and then screened for RFLPs by Southern hybridization with genomic fragments that spanned the region. The following three RFLPs were identified: a *Hin*dIII RFLP using a 700-bp PCR fragment from the *vermilion* coding sequence (Searles *et al.* 1990; primers VerA, 5′ GAACCGAGT GGTTCTGATTCT 3′; VerB, 5′ AACGAGTCGATGTCCATGAG 3′), a *Bgl*II RFLP using a 5-kb *Sal*I fragment from the K4.8.1 genomic clone, and *Bam*HI RFLP using a 4-kb *Bam*HI fragment from the K3.18.2 genomic clone. Upon identification of an RFLP, each of the 23 recombinant lines were screened to determine which form of the RFLP, *vermilion* or *sbr^{mgln}*, they carried.

Sequencing the *sbr* alleles: Examination of sbr^{1}, sbr^{ts148}, and sbr^{10} for possible sequence alterations was accomplished by sequencing the *sbr* cDNA obtained from homozygous adults of each genotype. For sbr^{ts148} and sbr^{10}, adults were obtained by raising the cultures at the permissive temperature of 18°. In addition to the sequence changes reported in results, there are also sequence polymorphisms that do not alter the protein sequence: a C to T change at nucleotide 1465, C to G at nucleotide 1479, and A to G at nucleotide 1503. To sequence the *sbr^{mgln}* lesion, we were forced to obtain the *sbr* cDNA from adult females heterozygous for *sbr^{mgln}* and another mutation, *sbr^{ts148}*. This was done because *sbr^{mgln}*'s lethality prevented us from obtaining homozygous adults, so we had to obtain the *sbr^{mgln}* cDNA from a mixed population of chromosomes. *sbr^{ts148}* was used as the second chromosome because the sequence lesion from this mutant had been identified first and it permitted the unequivocal identification of *sbr* cDNAs transcribed from the *sbr^{ts148}* chromosome. Any cDNA that did not carry the *sbr^{ts148}* mutation was considered to be from the *sbr^{mgln}* chromosome. We purified mRNA from 30 adult females of the genotype *sbr^{mgln}/sbr^{ts148}*, using a mRNA micropurification kit (Amersham, Arlington Heights, IL). Total adult cDNA was made from this mRNA preparation, using a first-strand synthesis kit (Amersham). PCR primers were designed within the 5′ and 3′ UTR (CBS11-Xho, 5′ CCTCGAGGAAGTTGGCA GCAGTTTGTG 3′; CBS11-R1, 5′ GGAATTCCATTATGTGGAT GTGGCACGC 3′) of *sbr* and used to amplify the full-length cDNA. The resulting PCR products were cloned into the pCRII vector [Invitrogen (San Diego) TOPO TA kit] and sequenced with a primer (CBS11-2970, 5′ CGATGGGACGAGGATGAT GAC 3′) that read through the T to A mutation at nucleotide 461 in the *sbr^{ts148}* cDNA. Two cDNAs from independent PCR reactions were shown not to contain the *sbr^{ts148}* mutation. These were fully sequenced to identify the lesion in *sbr* from the *sbr^{mgln}* chromosome.

RESULTS

We identified a new allele of *sbr* in a screen for X chromosome mutations that affect the pathfinding of embryonic motor neurons (Korey *et al.* 1997). After extensive mapping of this mutant, *magellan* (see below), we found that it was allelic to *sbr* and renamed the mutant *sbr^{mgln}*.

Axonal defects in *small bristles*: The neuromuscular system of the Drosophila embryo has been well characterized at the cell biological level (Bate and Broadie 1995). The intersegmental and segmental nerves (ISN and SN) are the two main motor nerve roots that exit the Drosophila central nervous system (CNS). In the periphery, these axon bundles divide into five branches that innervate the 30 body wall muscles in each hemisegment, as observed with the anti-Fasciclin II antibody mAb 1D4 (Van Vactor *et al.* 1993). The ISN innervates dorsal muscles and generates the ISNb and ISNd branches that innervate ventral muscles, whereas the SN pathway divides into SNa and SNc, which innervate lateral and ventral muscles, respectively (Figure 1A).

In *sbr* mutant embryos, we observe guidance defects in all motor axon pathways. With the exception of a viable hypomorph, *sbr^{1}*, lethal *sbr* alleles can be organized in an alleleic series of increasing severity of embryonic phenotypes. In general, *sbr* mutant axons extend but fail to follow the correct pathway to their targets (Figure 1). The most penetrant axonal defects are seen in the ISNb motor pathway, ranging from 54% of segments in weaker alleles to 80% of segments in the strongest alleles (Figure 1E). ISNd is also routinely absent from its target muscles, presumably due to failed defasci-

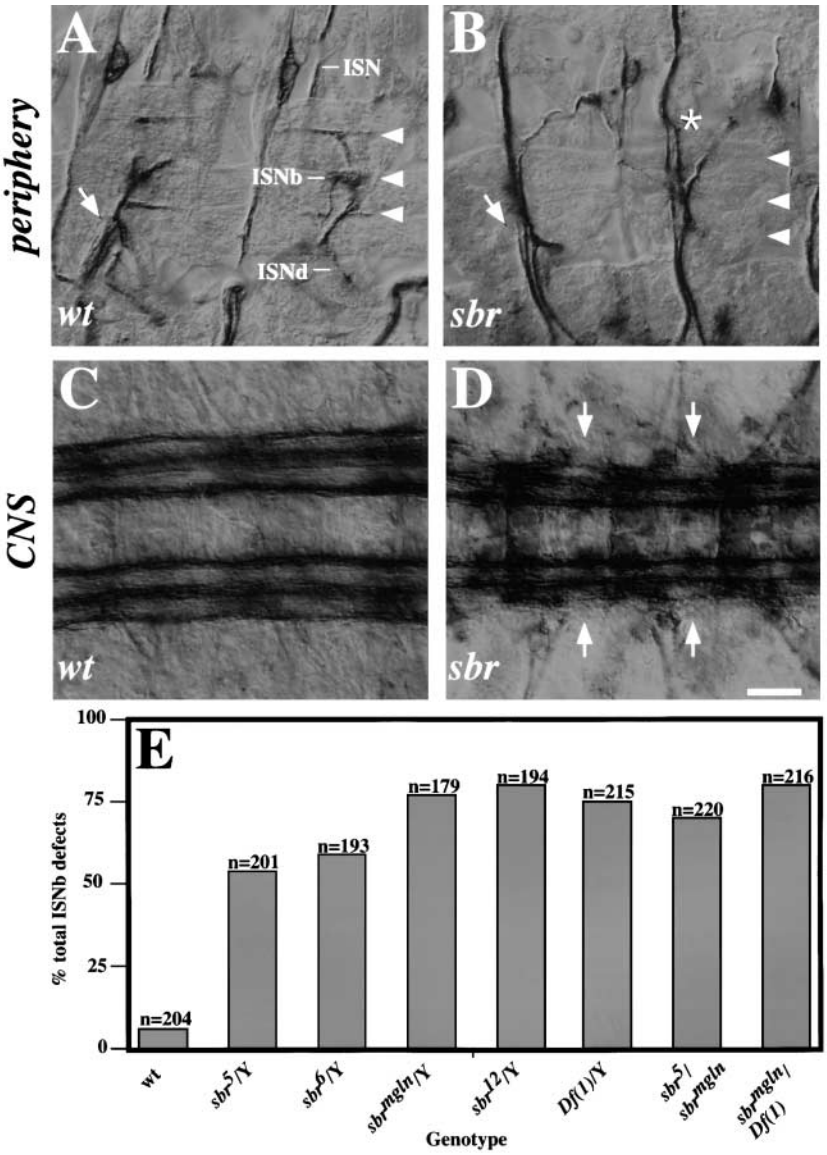

FIGURE 1.—Axon phenotypes in *small bristles* embryos. Images of a wild-type embryo and a *small bristles* embryo. Embryos were stained with mAb 1D4 and dissected to visualize the ventral muscle domain. Each image consists of two adjacent segments from stage 16–17 embryos with the arrow denoting the point at which ISNb enters the ventral muscle region. (A) Arrowheads identify the positions of the three stereotyped connections that are made by ISNb; two wild-type segments are shown. (B) An image of two sbr^{mgln} segments in which ISNb axons have passed by the ventral muscle region. The ISNb fascicle is marked with an asterisk. Arrowheads identify the three stereotyped connections that are made by wild-type ISNb axons. (C and D) Images of the CNS from a St16-17 wild-type and sbr^{mgln} embryo with arrows denoting breaks in the outermost fascicle. Embryos were stained with mAb 1D4 and dissected to visualize the ventral nerve cord. (C) Wild type; (D) sbr^{mgln}; (E) a graph of the total percentage of ISNb pathfinding errors observed in *sbr* embryos compared to a wild-type control. Pathfinding errors included both bypassing the ventral target muscles and entering the ventral target region and then subsequently failing to make the appropriate connections. *n*, number of hemi-segments (A2–A7); *Df(1) = Df(1)v-L4*. Bar, 5 μm.

culation from the ISN. In addition, we see a low penetrance crossing of the segment boundary by ISN in the dorsal regions of the embryo and variable defects in SN motor axon bundles. The alleles sbr^{mgln} and sbr^{12} display severity equivalent to a complete deletion of the gene, suggesting that they are functional nulls; although no antibody is available to confirm this prediction, sequence of sbr^{mgln} reveals a truncation of the predicted protein (see below). Careful examination of muscle cells in these strong alleles also reveals defects in muscle morphogenesis (see below). Although the peripheral motor axon pathfinding problems in *sbr* mutants could be secondary to these muscle defects, we also observe axonal defects within the CNS neuropil where muscle cell morphogeneisis is unlikely to affect axonogenesis.

The ventral nerve cords of *sbr* mutants show highly penetrant defects in the development of the longitudinal axon scaffold as revealed by mAb 1D4 (Figure 1, C and D). This antibody highlights three parallel Fasciclin II-positive fascicles on either side of the ventral midline. In *sbr* embryos, the outermost fascicle contains frequent gaps or is thinner than normal, a phenotype common to many mutations in axon guidance genes (*e.g.* integrin subunits, HOANG and CHIBA 1998; *dTrio*, BATEMAN *et al.* 2000). This phenotype may be the result of defective interaxon communication that obstructs axon extension or fasciculation in the longitudinal pathways.

Since axonal phenotypes can represent secondary consequences of defective cell fate determination, we also examined the pattern of embryonic CNS cell fates. We stained *sbr* embryos with several nuclear markers including antibodies to Engrailed (data not shown) and Even-skipped proteins (Figure 2). Our analysis demonstrates that the number and position of cells expressing each of these markers appears normal in sbr^{mgln} embryos, suggesting that the axon guidance phenotypes we observe are a result of later defects in differentiation and morphogenesis.

Embryonic muscle defects: After examining the defects in motor axon and CNS pathfinding, we noted

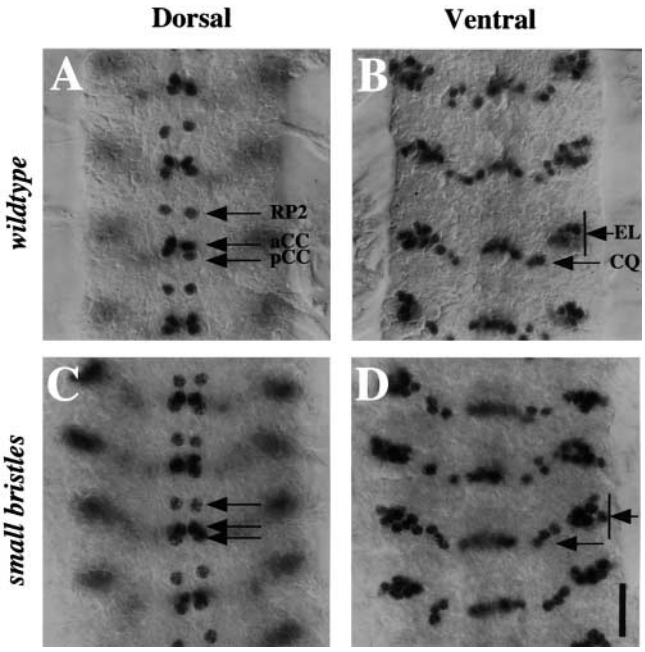

FIGURE 2.—Even-skipped cell fate analysis. Images of the dorsal and ventral focal planes of the ventral nerve cord of stage 16–17 embryos. (A and B) Images of a wild-type control embryo. In the dorsal view, RP2, aCC, and pCC are visible and labeled. In the ventral plane, the EL and CQ neurons are visible and labeled. The arrows in subsequent images reference the wild-type neurons labeled. (C and D) Images of sbr^{mgln} ventral nerve cords. Bar in D, 10 μm.

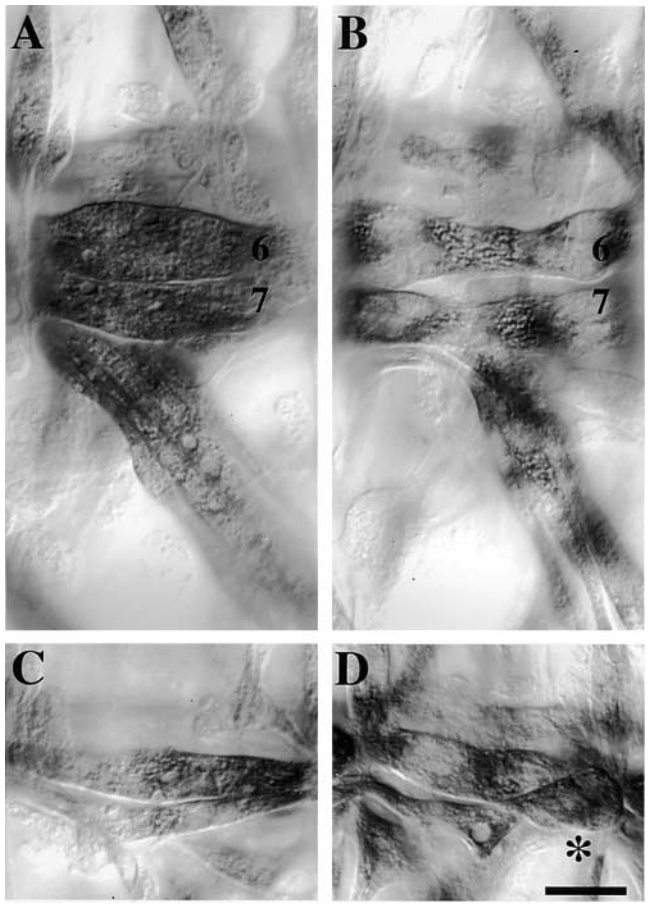

FIGURE 3.—Embryonic muscle defects in *small bristles* mutants. Shown are muscles from stage 16 embryos stained with mAb FMM5, which recognizes the myosin heavy chain. (A) An image of one segment of a wild-type stage 16 embryo showing the ventral and oblique muscle fields. Muscles 6 and 7 are shown in this plane of focus. (B) An image similar to that shown in A from a sbr^{mgln}/sbr^{12} embryo. The image shows the change in myosin localization and the change in morphology of these muscles. (C) An image of muscles 6 and 7 from a sbr^{mgln}/sbr^{5} embryo showing the morphology defects in these muscles. (D) An image of a sbr^{mgln}/sbr^{6} embryo showing a muscle (likely to be muscle 7) that has pulled out of its insertion site (asterisk). Bar in D, 8 μm.

that there also appeared to be defects in the morphology of the body wall muscles in the strongest alleles. The embryonic musculature begins to develop as the germ band shortens around stage 12 of embryonic development (BATE 1990). Initially, muscle precursors or founder cells develop for each specific muscle, which then recruit surrounding myoblasts to fuse and form fully differentiated multinucleate muscle. As each muscle cell grows it also elongates and sends out processes to find and insert at a specialized epidermal muscle attachment site. By stage 15–16, all 30 of the individual abdominal muscles have been formed in each segment (BATE 1990).

In *sbr* embryos, we find that the muscles appear to have initially differentiated correctly, forming the correct number of muscles in the right positions in each segment. However, at stage 16, these muscles have an aberrant morphology including long drawn out fibers (Figure 3) and in some cases muscles appear to have pulled out of their epidermal attachment site (Figure 3D). These phenotypes are consistent with problems associated with late muscle morphogenesis suggestive of defects in cytoskeletal and other structural components that form the fully functional contractile apparatus. Consistent with this hypothesis, staining with an antibody that recognizes the myosin heavy chain reveals a disrupted pattern of myosin localization and reduced levels of the antigen (Figure 3). It is possible that, given the described defects of the musculature, problems in the target field could explain the motor axon pathfinding errors, but not those within the CNS.

Germline clones of *sbr* are germline lethal: While *sbr* zygotic mutations affect the development of both the motor neurons and the body wall muscles, this does not address whether *sbr* has an earlier role in embryonic development. It is likely that maternal expression of *sbr* allows embryos to reach late stages of embryonic development (see below). To address this question, we made germline clones with the sbr^{mgln} allele using the FLP/FRT recombination system and the dominant female sterile mutation ovo^{D1}.

Germline clones with the sbr^{mgln} chromosome produce sterile females (n = 180 females) that fail to lay eggs. The wild-type chromosome control was completely fer-

tile (n = 150 females), laying eggs that hatched into adults. We dissected the ovaries from heat-shock-treated *y w sbr^{mgln}* FRT101/ *ovo^{D1}* FRT101 females (mutant, n = 67) and *y w* FRT101/ *ovo^{D1}* FRT101 females (control) and found that the *sbr^{mgln}* clones had no discernible egg chambers present, suggesting that there is probably an earlier defect in ovary development. This result prevents us from addressing the early embryonic role of *sbr*.

***sbr* mutations affect macrocheate development:** The *small bristles* mutation was named for its affect on the large sensory bristles present on the thorax and head of the Drosophila adult (Lindsley and Zimm 1992). These bristle cells are part of a sensory system of small (microchaete) and large (macrochaete) bristles that cover the insect's exoskeleton. Along with the bristle cell, there are three associated cells: a supporting socket cell, a neuronal cell that extends a process into the bristle shaft, and a glial cell. These four cells differentiate from a single progenitor sensory organ precursor cell present in the larval imaginal wing discs (reviewed in Simpson *et al.* 1999). Once the cell types have been specified, the bristle cell extends a process between 32 and 48 hr of pupal development, which will become the sensory bristle. Within each macrochaete, 16–25 hexagonally arrayed bundles of actin run the length of the bristle attached to the cell membrane (Tilney *et al.* 1996). These filaments, made of repeated modules of actin filaments (Tilney *et al.* 1996), are thought to play a key role in bristle extension because inhibitors of filament assembly slow growth *in vitro* while filament stabilizers accelerate growth (Tilney *et al.* 2000). The outward manifestation of the actin bundles in fully developed bristles is a distinct ridging pattern produced by the cell membrane protruding out between two actin bundles (Tilney *et al.* 1996). Upon full extenision of the bristle, the cuticle is secreted to support the cell and the actin filaments are degraded to produce a hollow bristle in which the sensory axon process extends. In contrast to the actin cytoskeleton, the microtubules that fill the cytoplasm of the bristle throughout development do not play a role in extension (Tilney *et al.* 2000). Instead, they may provide cytoplasmic bulk to the bristle, similar to the role intermediate filaments play in other systems (Tilney *et al.* 2000).

The adult viable *sbr^{1}* mutation was first isolated on the basis of its bristle phenotype (Lindsley and Zimm 1992), but a detailed analysis of the defects in bristle formation was not performed. In different alleleic combinations of the *sbr^{1}* allele with lethal *sbr* alleles, adults have smaller than normal macrochaetes when compared to wild type while the smaller microchaetes appear grossly normal (Figure 4, A–E). Scanning electron microscopy of the macrochaete surface shows that the bristles are smaller in diameter, while the external ridging is reduced in number and is less distinct in *sbr* mutants (Figure 4, F–H). The ridging is further reduced in stronger allelic combinations and in some cases the bristle cell does not extend out of the socket cell (Figure 4I) or occasionally the bristle and socket cells are absent altogether (Figure 4C). Furthermore, notal clones made with the *sbr^{mgln}* chromosome, which behaves as a null, cause bristles to be severely reduced in size or absent (data not shown). Consistent with the ridging adding strength to the bristle structure (much like corrugated metal sheeting) we observe large numbers of broken bristle shafts in *sbr* adults (Figure 4J). In summary, the decreased bristle length and diameter, the loss of ridging, and the absence of bristles from socket cells suggest

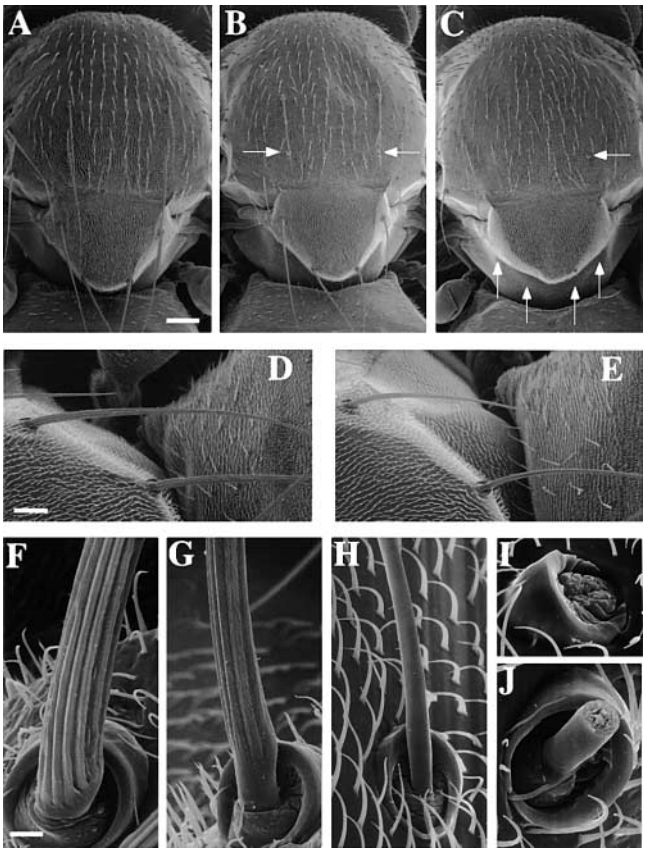

Figure 4.—SEM of sensory bristles from *small bristles* mutants. (A) A wild-type notum at 100× magnification showing the small microchaetes and the larger macrocheates. (B) A *sbr^{1}* notum showing shortened and missing (arrows) macrochaetes (100× magnification). (C) A *sbr^{5}*/ *sbr^{1}* notum (100× magnification). The stronger allelic combination produces smaller bristles and causes more to be missing altogether (arrows). (D) An image of a wild-type scutellar bristle at 300× magnification. (E) An image of the same scutellar bristle in a *sbr^{1}* mutant showing the decrease in length. (F) A 2000× magnification image of the base of a wild-type macrochaete showing the distinct ridging present on the bristle cell surface. (G) An image of a *sbr^{1}* macrochaete (2000×) showing the decrease in external ridging and the decrease in diameter. (H) An image of a *sbr^{mgln}*/ *sbr^{1}* macrochaete (2000×) showing an increased loss of ridging and the severe decrease in diameter present in this genetic combination. (I) A close-up of a *sbr^{mgln}*/ *sbr^{1}* socket from which no bristle appears to have elongated. (J) An image of a broken bristle from an *sbr^{mgln}*/ *sbr^{1}* adult. Bars: 100 μm (A), 50 μm (D), and 15 μm (F).

that there are defects in the underlying cytoskeleton. The common theme of defects in the structure and morphogenesis of neural, muscle, and epidermal tissues in *sbr* mutants encouraged us to identify the gene encoded by this locus.

Genetic mapping of the *small bristles* locus: We began the initial mapping with the strong EMS-induced allele sbr^{mgln} that we obtained in a screen for axon guidance mutants. Recombination mapping with a *y m wy sd os* chromosome placed sbr^{mgln} approximately one chromosomal division from *miniature* (*m*, 10E1–2) while mapping with a *y cv v f car* chromosome suggested that the lesion was extremely close to *vermilion* (*v*, 10A1–2). On the basis of these initial results, we performed a high-resolution recombination mapping analysis between the sbr^{mgln} lesion and *vermilion*. This analysis produced a recombination distance of 0.28 cM, which translated into a physical distance of ~94.2 kb between sbr^{mgln} and *v* (based on 0.01 cM = 3.3 kb in this region; Kozlova *et al.* 1994). This distance implies that the sbr^{mgln} lesion lies on or near the end of the previously published Zhimulev genomic walk through the *vermilion* region (Figure 3-1C, Kozlova *et al.* 1994). The mapping of our allele to this chromosomal position was consistent with previous genetic mapping of the *sbr* locus (Zhimulev *et al.* 1981b). Subsequent genetic complementation assays confirmed that our new lethal mutation is a strong allele of *sbr*.

In parallel to the recombination mapping and the previous work on this locus, duplication and deficiency chromosomes were also used to identify the region of the X chromosome affected by the sbr^{mgln} lesion. We identified a duplication, *Dp(1;y)v+y+* (Zhimulev *et al.* 1981a), which cleanly rescued normally lethal sbr^{mgln} males to complete viability and fertility. This duplication permitted us to use deficiencies to locate the *sbr* interval on the X chromosome. Consistent with previous *sbr* work (Zhimulev *et al.* 1981b), we found that Df(1)v-L15 and Df(1)v-L4 failed to complement sbr^{mgln} lethality, while Df(1)HC133 and Df(1)v-L3 were viable when heterozygous with the sbr^{mgln} lethal. Consistent with the mapping of lethality, both Df(1)v-L15 and Df(1)v-L4 (Figure 1E) showed phenotypes specific to *sbr*, both alone and when heterozygous with *sbr* alleles. The deficiencies Df(1)HC133 and Df(1)v-L3 did not. On the basis of published breakpoint analysis of these deficiencies, the *sbr* locus was determined to be within the 9F5–9F10 interval of the X chromosome (Zhimulev *et al.* 1981a).

Molecular mapping of *small bristles*: To identify the *sbr* open reading frame, we took two parallel approaches to correlate the genetic and physical maps: recombination mapping with RFLP markers and deficiency breakpoint mapping. The high-resolution recombination mapping between the sbr^{mgln} allele and *vermilion* (*v*) produced 23 lines with independent recombination events between the sbr^{mgln} lesion and *v* (representing a total of 72 recombinants out of 25,276 F_2 progeny). Using genomic phage clones from the Zhimulev walk, we identified three RFLP markers in the 100-kb interval between *v* and sbr^{mgln} (see MATERIALS AND METHODS). The recombinant lines were then screened for the enzyme cutting pattern characteristic of either sbr^{mgln} or *v*. The frequency at each site was plotted *vs.* the physical distance on the chromosome to predict the intercept at 0% recombination and therefore the location of the sbr^{mgln} lesion (Figure 5A). An approximate degree of accuracy was estimated by dividing the approximate sbr^{mgln} to *v* physical distance of 100 kb by the 23 independent recombinant lines, giving a resolution of nearly 5 kb on either side of the intercept.

The intercept bisected the 3′ end of an open reading frame encoding the DmNXF1 protein, but it was also close to an open reading frame encoding the Drosophila homolog of the RNA-binding protein Vera (*dIMP*; Figure 5B). To obtain independent evidence that *sbr* encodes the DmNXF1 protein, we mapped the deficiency breakpoints that most closely defined the *sbr* locus. The complementing Df(1)HC133 was found to break in the 5′ UTR of *dIMP* and remove the complete open reading frame (Figure 5B). Consistent with the mapping, this deficiency also eliminates the embryonic expression of the *dIMP* gene (data not shown). We then found that the proximal breakpoint of the complementing deletion Df(1)vL3 lies within a 5-kb fragment that includes the 5′ end of DmNXF1 (Figure 5B). Since identified mutations in DmNXF1 [sbr^{ts148}, sbr^{10} (G. Wilkie and I. Davis, personal communication), and sbr^{mgln} (this article)] complement this deficiency, Df(1)vL3 does not remove *sbr*. Finally, we found that Df(1)v-L4 breaks just outside of the DmNXF1 3′ end and removes the entire DmNXF1 coding region (Figure 5B). Thus, the three techniques we used, recombination mapping, deficiency mapping, and RFLP mapping, all strongly and independently point to DmNXF1 as the protein encoded by *small bristles*.

In light of this we identified a cDNA encoding the full-length *sbr* open reading frame from a mixed-stage poly(A)$^+$ selected embryonic cDNA library. After sequencing the full-length cDNA and comparing it to the Berkeley *Drosophila* Genome Project genomic sequence, we found that the *sbr* genomic region has 10 exons and encodes a 672-amino-acid protein, DmNXF1 (accession numbers: protein, CAB64382; nucleotide, AJ251947), which retains the conserved domain structure when aligned with the human and yeast homologs (Figure 6A; Herold *et al.* 2000). The RNA-binding domain, the leucine rich repeats, the NTF2-like domain, and the UBA-like domain including the 3-amino-acid nucleoporin binding NWD motif are all present in the Drosophila homolog (Herold *et al.* 2000). Northern analysis on total embryonic RNA shows that it is maternally loaded (data not shown) and is expressed highly during embryonic development (Figure 6C). *In situ* analysis indicates

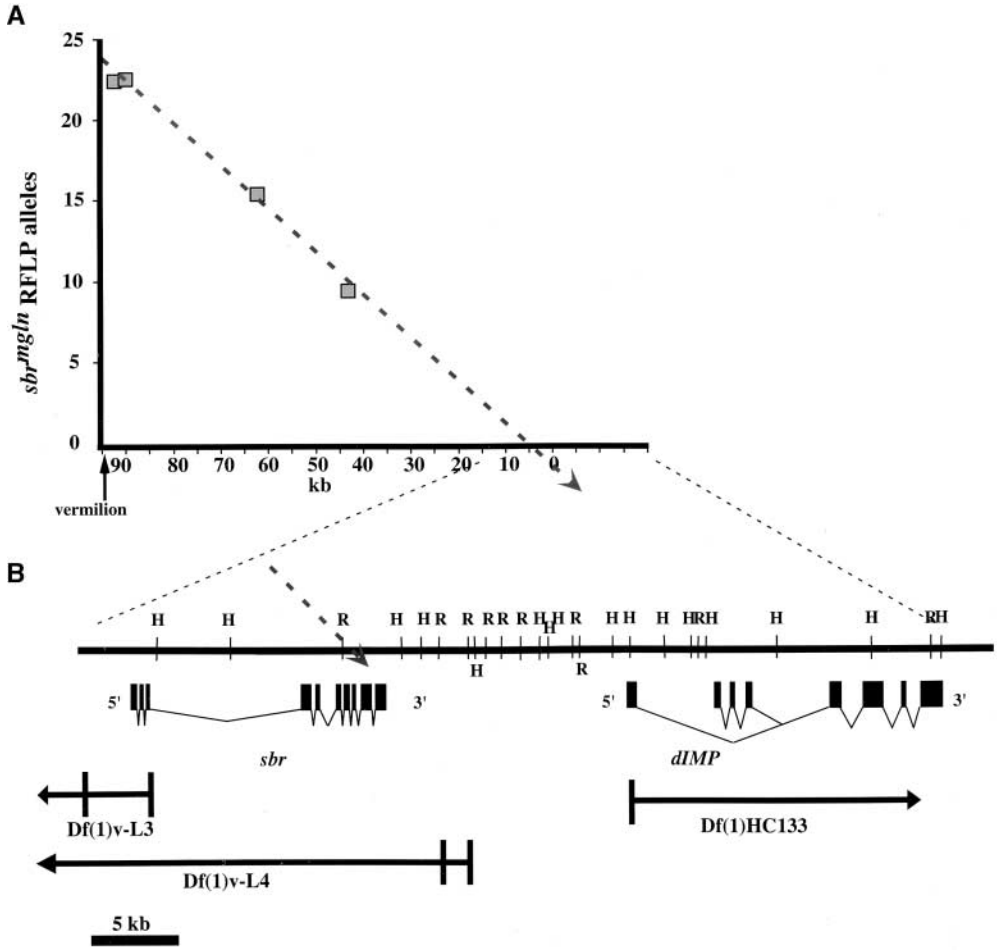

FIGURE 5.—RFLP and deficiency mapping of *small bristles*. (A) A graph of the RFLP data generated in this study. Each RFLP (shaded boxes) identified was plotted on a graph of the genomic distance from vermilion *vs.* the number of the 23 recombinant lines that showed the sbr^{mgln} form of the RFLP. A best-fit line was produced using Cricket Graph with the *x*-intercept being the location of the lesion on the sbr^{mgln} chromosome. The distance in kilobases is labeled according to KOZLOVA *et al.* (1994), with the 0 point being the end of the walk described in that article. (B) A diagram of the *sbr* genomic region enlarged from the *x*-axis in A. The *sbr* and *dIMP* transcript maps are shown in relation to the identified deficiency breakpoints and the RFLP intercept. The DNA missing from the deficiency chromosomes is indicated by the solid horizontal lines, with the uncertainty in the breakpoints shown by the solid vertical lines. The RFLP intercept is placed on this genomic map bisecting the 3′ end of *sbr*.

that it is expressed ubiquitously at low levels throughout embryonic development (data not shown).

Sequencing *small bristles* lesions: Sequencing the hypomorphic sbr^{1} allele revealed no sequence changes within the DmNXF1 open reading frame, suggesting that the defects we see may be due to a hypomorphic mutation within a promoter or enhancer for this gene. This is consistent with the weak nature of the allele and the limitation of the phenotype to sensory bristles. sbr^{ts148} has a T to A mutation at nucleotide 461, causing a valine to glutamic acid change at residue 154 within the RNA-binding domain of the protein (see solid box in Figure 6A). sbr^{10} has a C to T mutation at nucleotide 416, causing a proline to leucine change at residue 139, also within the RNA-binding domain of the protein. There are also two mutations in sbr^{10} that produce conservative changes: threonine to serine at position 493 (A to T at nucleotide 1477) and methionine to isoleucine at residue 499 (G to T at nucleotide 1497; see solid circles in Figure 6A; also see MATERIALS AND METHODS).

The initial amplification of the sbr^{mgln} cDNA showed an upward band shift of the cDNA in relation to the wild-type sequence, indicating that the mutant form was larger. Sequencing of the sbr^{mgln} cDNA reveals a 67-bp insertion within the coding region of DmNXF1. When further analyzed, the inserted sequence was identified as the intron between exons 7 and 8. The failure to splice out the intron is due to a point mutation that changes the conserved 5′ splice site of intron 7 from GT to AT (Figure 6B). The retention of the intron produces a premature stop codon that terminates the protein at amino acid 417 (see asterisk in Figure 6A) and removes the conserved C terminus of the protein, including part of the NTF2-like domain and the UBA-like domain (Figure 6). Sequencing of the genetic background that was used to produce this mutant does not show this sequence alteration. This mutation does not prevent transcription of the gene since we were able to obtain full-length mutant cDNA. Thus, the mutation affects *sbr* post-transcriptionally by producing an unstable mRNA, a truncated form of the protein that is unstable and degraded, or a form of the protein that is unable to perform its normal cellular functions.

DISCUSSION

The analysis of *small bristles* mutants and our subsequent cloning of the locus provides a unique opportunity to analyze the *in vivo* role of mRNA export during Drosophila development. We found that mutations in

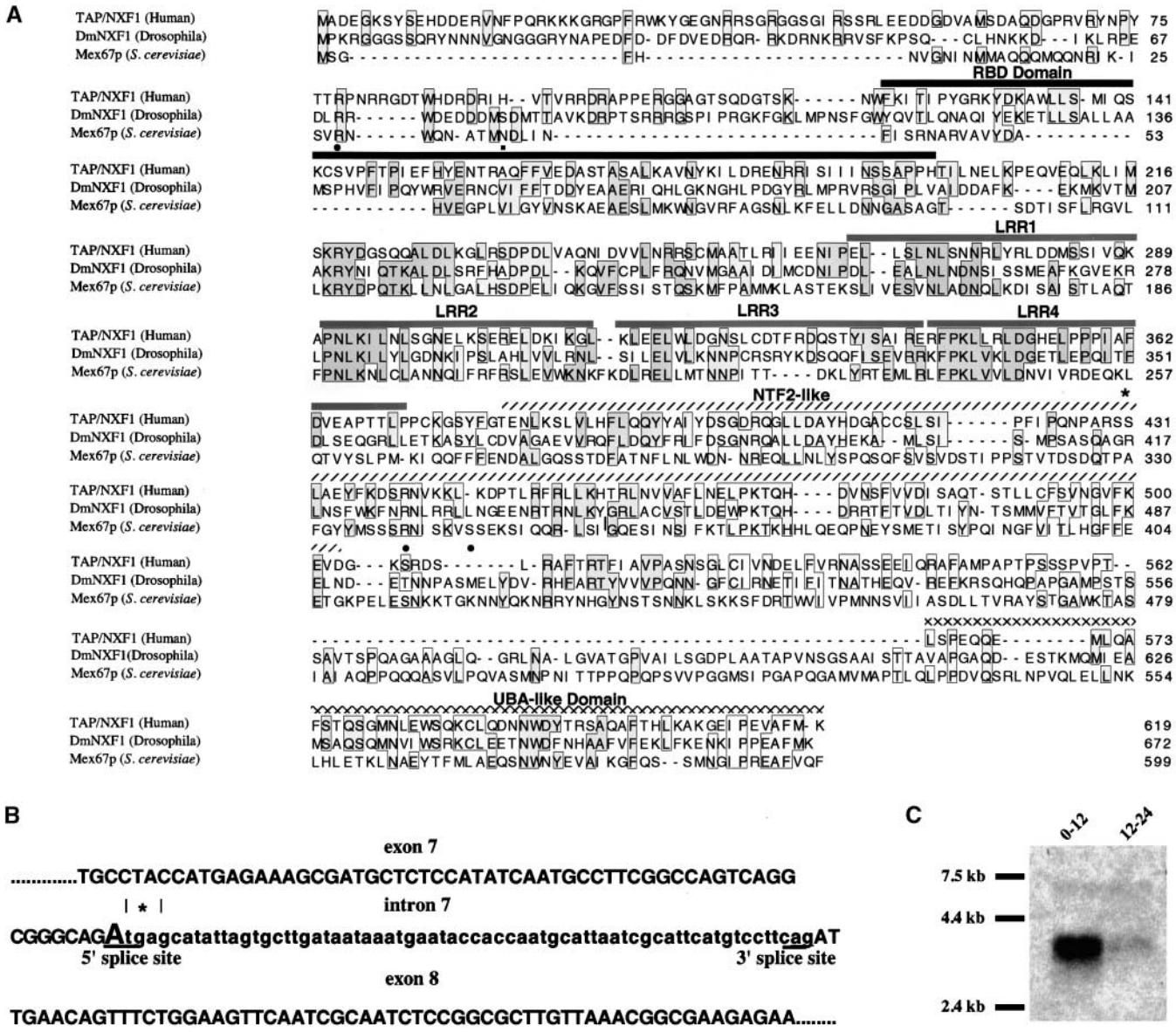

FIGURE 6.—*small bristles* encodes *DmNXF1*. (A) An alignment of the protein sequences of human TAP/NXF1, the yeast Mex67p, and DmNXF1. Identical residues are shaded. The domain structure of DmNXF1 is labeled above the sequence alignment with each of the domains labeled according to HEROLD *et al.* (2000). RBD, RNA-binding domain; LRR, Leucine rich repeat; UBA, ubiquitin associated. The solid box labels the position of the valine to glutamic acid change at residue 154 in sbr^{ts148}. The solid circles label the position of the proline to leucine change at residue 139 and the two conservative changes, threonine to serine at position 493 and methionine to isoleucine at residue 499, in sbr^{10}. The asterisk labels the point in the sbr^{mgln} allele where the protein is truncated by a premature stop codon. (B) A diagram of the point mutation identified in the sbr^{mgln} allele. The parts of exons 7 and 8 shown are in uppercase letters while the intervening intron is lowercase. The G to A mutation is shown as a large A while the premature stop codon produced is labeled with an asterisk. The 5′ and 3′ splice sites are underlined. (C) A Northern blot indicating the expression of *sbr* during embryonic development, which shows its expression in embryos collected at 0–12 and 12–24 hr of embryonic development.

small bristles affect the morphogeneis of embryonic neurons, embryonic muscle, and adult sensory bristles. We have shown that *sbr* encodes the DmNXF1 protein, the Drosophila homolog of a mRNA export protein that has been characterized in human (TAP/NXF1) and yeast (Mex67p). In these systems, this family of proteins has been shown to play a major role in the export of mRNA from the nucleus to the cytoplasm. We have shown that DmNXF1 has similar domain structure to its homologs (Figure 6A), and *sbr* embryos display defects in the export of mRNA out of the nucleus (G. WILKIE, C. A. KOREY, D. VAN VACTOR and I. DAVIS, unpublished results). Furthermore, DmNXF1 is required for mRNA export in SL2 cells (A. HEROLD and E. IZARRAULDE, personal communication). Together these studies show that function of the Drosophila homolog

is consistent with its role as a major mRNA export protein in other systems.

Our analysis of developmental defects in *sbr* mutants suggests that the phenotypes we observe are not the result of cell fate problems, but rather are due to problems in late-stage differentiation and cell morphogenesis. The following question remains: Knowing the cellular function of *sbr*, how are the pathfinding of neurons, the structural integrity of muscles, and the development of the bristle related? Given that a global decrease in mRNA export in these mutants is likely, the phenotypes suggest that certain tissues are more sensitive to the lower levels of mRNA and the resultant decrease in protein synthesis. This hypothesis is consistent with work on the *Minute* syndrome in Drosophila. This collection of phenotypes is associated with >50 different loci throughout the genome. The *Minutes* are usually haploinsufficient and produce a variety of phenotypes, including delayed larval development, recessive lethality, short and thin bristles, and reduced fertility and viability (reviewed by Lambertsson 1998). The recent identification of the genes encoded by several *Minute* loci has shown that many are mutations in ribosomal proteins (Lambertsson 1998), suggesting that the phenotypes observed are a result of defective protein synthesis.

It has been proposed that the specific cell types affected represent tissues that require large amounts of protein synthesis during development (Lambertsson 1998). For example, both the rapid extension of sensory bristles and gametogenesis are dependent on the precise synthesis of necessary proteins. Placed in this context, there is significant overlap between the phenotypes we observe in *sbr* mutants and the *Minute* mutations. While *sbr* does not appear to be haploinsufficient, we have shown that *sbr* loss-of-function mutants have smaller and thinner bristles and are defective in the development of the female germline. Other alleles of *sbr* have defects in spermatogenesis and decreased viability (sbr^{17}, Dybas *et al.* 1983). This framework may explain the defects we see both in the embryo and the adult.

The development of the bristle is thought to require a rapid synthesis of proteins (Mitchell *et al.* 1977). The hypomorphic sbr^{1} allele permitted us to examine the effect of stronger *sbr* alleles in the adult. The loss of ridging and significantly reduced length in *sbr* mutants is consistent with a defect in the bristle cell actin cytoskeleton, while the decreased diameter of the bristles may indicate a decrease in the number of microtubules (Tilney *et al.* 2000). A defect in the export of actin, tubulin, and other required mRNAs could reduce the available pool of these proteins, thereby decreasing the bristle cells' ability to initiate and rapidly extend. Furthermore, we see gross defects only in the larger macrochaetes, while the much smaller microchaetes appear relatively normal. Although they are different in size (250 μm compared to 70 μm), they develop over the same period of time, indicating that macrochaetes grow at a significantly greater rate (Tilney *et al.* 2000). Consistent with their larger size, macrochaetes also have more actin bundles (16–25 bundles *vs.* 7–11 bundles in microchaetes) with each bundle containing more actin filaments (Tilney *et al.* 2000). Taken together this suggests that macrochaetes require a greater rate of protein synthesis and polymer assembly during development, possibly sensitizing them to a loss of essential mRNAs.

Similar to bristle cells, muscle cells also require large amounts of protein to construct a fully functional contractile apparatus. The cytoplasm of a fully developed muscle is filled with actin, myosin, and other supporting structural proteins. To address the genetic requirements of a developing muscle, several laboratories have done dominant flightless screens (Mogami and Hotta 1981; Cripps *et al.* 1994). These screens have shown that mutations in myosin and actin are haploinsufficient for the correct development of the adult indirect flight muscles. Several of the recovered mutations are loss-of-function alleles (Mogami *et al.* 1986; Cripps *et al.* 1994), suggesting that development of these muscles is sensitive to gene dose. Although these mutations do not appear to be haploinsufficient in the embryo (Mogami *et al.* 1986), the requirement for these proteins in the embryonic musculature is likely to be the same. We showed that zygotic mutations in *sbr* produce morphological defects in the body wall muscles that are similar to those reported in muscle protein loss-of-function mutants (*i.e.*, MSP-300, Rosenberg-Hasson *et al.* 1996; Laminin, Volk and Yarnitzky 1995; and Tiggrin, Bunch *et al.* 1998). The defects we observe are consistent with a failure to develop a structurally sound contractile apparatus and insertion site. Supportive of this hypothesis, we show a failure to properly distribute myosin throughout the muscle cytoplasm. Similar to the bristle extension defect, this phenotype is consistent with a decrease in the available protein pools as a result of defective mRNA export from the nucleus to the cytoplasm.

The defects in morphology of the muscles as well as the possible decrease in relevant muscle-derived guidance factors could be the cause of the misdirected motor axons. This is seen in *abrupt* embryos, where ISNb pathfinding errors and a low frequency of muscle insertion site pullouts are observed. *Abrupt*'s identity as a muscle-expressed zinc finger protein that potentially functions as a transcription factor suggests that the loss of certain muscle proteins can produce both axon and muscle defects (Hu *et al.* 1995). However, this would not explain the axon pathway defects we observe in the developing embryonic CNS.

As with muscles, a general decrease in specific guidance molecules in the developing embryo could impair growth cone navigation. However, it also could disrupt the machinery required to drive the growth cone forward. Treating growth cones with drugs that disrupt the actin cytoskeleton disrupts the structure of the growth cone and causes navigational errors *in vivo* (Bentley

and Toroian-Raymond 1986; Chien *et al.* 1993; Kaufmann *et al.* 1998). In the Drosophila embryo, injection of cytochalasin at low doses where motility is preserved produces bypass phenotypes similar to those observed in *sbr* mutants (Kaufmann *et al.* 1998). Thus, the axon pathway defects in *sbr* mutants may reflect a partial decrease in actin assembly due to a reduced supply of certain key components.

Work on neurites *in vitro* has shown that actin mRNA is transported along axons in particles to the growth cone (Bassell *et al.* 1998). Furthermore, application of neurotrophin to growth cones *in vitro* produces an increase in actin polymerization at the leading edge as well as the localization of actin mRNA to the growth cone (Zhang *et al.* 1999). Consistent with a functional role for localization, inhibition of actin mRNA localization to the leading edge of chicken embryonic fibroblasts reduces the rate of cell motility (Kislauskis *et al.* 1997). On the basis of these data, a model is forming that suggests maximum rates of motility and directed outgrowth in neurons may require the localization of actin mRNA and local translation of actin protein within the growth cone (Zhang *et al.* 1999). Thus, a decrease in mRNA export in *sbr* mutants may not decrease only the available pool of actin monomers at the growth cone; it may also decrease the presence of actin mRNA available for local synthesis during pathfinding, which could significantly impair the growth cone's directed motility.

We thank Andrea Herold and Elisa Izaurralde for communicating unpublished data and commenting on our manuscript. We also thank Igor Zhimulev for genomic phage clones and fly lines, William Fowle for technical assistance with SEM, and the members of the Van Vactor and Flanagan Labs for helpful discussions at all stages of this work. This work was supported by a National Institutes of Mental Health Predoctoral NRSA (C.A.K.), National Institutes of Health grants NS40043 and NS35909, a Wellcome Trust career development fellowship (I.D.), a Lister Institute senior fellowship (I.D.), and an MRC studentship (G.S.W.). C.A.K. was a National Science Foundation predoctoral fellow and D.V.V. is a Leukemia and Lymphoma Society scholar.

LITERATURE CITED

Bachi, A., I. C. Braun, J. P. Rodrigues, N. Pantè, K. Ribbeck *et al.*, 2000 The C-terminal domain of TAP interacts with the nuclear pore complex and promotes export of specific CTE-bearing RNA substrates. RNA **6:** 136–158.

Bassell, G. J., H. Zhang, A. L. Byrd, A. M. Femino, R. Singer *et al.*, 1998 Sorting of β-actin mRNA and protein to neurites and growth cones in culture. J. Neurosci. **18:** 251–265.

Bate, M., 1990 The embryonic development of larval muscles in *Drosophila*. Development **110:** 791–804.

Bate, M., and K. Broadie, 1995 Wiring by fly: the neuromuscular system of the *Drosophila* embryo. Neuron **15:** 513–525.

Bateman, J., H. Shu and D. Van Vactor, 2000 The guanine nucleotide exchange factor trio mediates axonal development in the *Drosophila* embryo. Neuron **26:** 93–106.

Bear, J., W. Tan, A. S. Zolotukhin, C. Tabernero, E. A. Hudson *et al.*, 1999 Identification of novel import and export signals of human TAP, the protein that binds to the CTE element of the type D retrovirus mRNAs. Mol. Cell. Biol. **19:** 6306–6317.

Bentley, D., and A. Toroian-Raymond, 1986 Disoriented pathfinding by pioneer neurone growth cones deprived of filopodia by cytochalasin treatment. Nature **323:** 712–715.

Braun, I. C., A. Herold, M. Rode, E. Conti and E. Izaurralde, 2001 Overexpression of TAP/p15 heterodimers bypasses nuclear retention and stimulates nuclear mRNA export. J. Biol. Chem. **276:** 20536–20543.

Bray, M., S. Prasad, J. W. Dubay, E. Hunter, K.-T. Jeang *et al.*, 1994 A small element from the Mason-Pfizer monkey virus genome makes human immunodeficiency virus type 1 expression and replication Rev-independent. Proc. Natl. Acad. Sci. USA **91:** 1256–1260.

Bunch, T. A., M. W. Graner, L. I. Fessler, J. H. Fessler, K. D. Schneider *et al.*, 1998 The PS2 integrin ligand tiggrin is required for proper muscle function in *Drosophila*. Development **125:** 1679–1689.

Chien, C. B., D. E. Rosenthal, W. A. Harris and C. E. Holt, 1993 Navigational errors made by growth cones without filopodia in the embryonic *Xenopus* brain. Neuron **11:** 237–251.

Cripps, R. M., E. Ball, M. Stark, A. Lawn and J. C. Sparrow, 1994 Recovery of dominant, autosomal flightless mutants of *Drosophila melanogaster* and identification of a new gene required for normal muscle structure and function. Genetics **137:** 151–164.

Dybas, L. K., K. K. Harden, J. L. Machnicki and B. W. Geer, 1983 Male fertility in *Drosophila melanogaster*: lesions of spermatogenesis associated with male sterile mutations of the vermilion region. J. Exp. Zool. **226:** 293–302.

Grüter, P., C. Tabernero, C. von Kobbe, C. Schmitt, C. Saavedra *et al.*, 1998 TAP, the human homolog of Mex67p, mediates CTE-dependent RNA export from the nucleus. Mol. Cell **1:** 649–659.

Herold, A., M. Suyama, J. P. Rodrigues, I. C. Braun, U. Kutay *et al.*, 2000 TAP (NXF1) belongs to a multigene family of putative RNA export factors with a conserved modular architecture. Mol. Cell. Biol. **20:** 8996–9008.

Hoang, B., and A. Chiba, 1998 Genetic analysis on the role of Integrin during axon guidance in *Drosophila*. J. Neurosci. **18:** 7847–7855.

Hu, S., D. Fambrough, J. R. Atashi, C. S. Goodman and S. T. Crews, 1995 The *Drosophila abrupt* gene encodes a BTB-zinc finger regulatory protein that controls the specificity of neuromuscular connections. Genes Dev. **9:** 2936–2948.

Hurt, E., K. Straber, A. Segref, S. Bailer, N. Schlaich *et al.*, 2000 Mex67p mediates nuclear export of a variety of RNA polymerase II transcripts. J. Biol. Chem. **275:** 8361–8368.

Katahira, J., K. Straber, A. Podtelejnikov, M. Mann, J. U. Jung *et al.*, 1999 The Mex67p-mediated nuclear mRNA export is conserved from yeast to human. EMBO J. **18:** 2593–2609.

Kaufmann, N., Z. P. Wills and D. Van Vactor, 1998 Drosophila Rac1 controls motor axon guidance. Development **125:** 453–461.

Kiehart, D. P., and R. Feghali, 1986 Cytoplasmic myosin from *Drosophila melanogaster*. J. Cell Biol. **103:** 1517–1525.

Kislauskis, E. H., X.-C. Zhu and R. H. Singer, 1997 β-Actin messenger RNA localization and protein synthesis augment cell motility. J. Cell Biol. **136:** 1263–1270.

Korey, C., C. Bascom-Slack, D. Scalice, B. Percival and D. Van Vactor, 1997 X-chromosome genes provide further insight into embryonic motor axon guidance (Abstr). Soc. Neurosci.

Kozlova, T. Y., V. F. Semeshin, I. V. Tretyakova, E. B. Kokoza, V. Pirrotta *et al.*, 1994 Molecular and cytogenetical characterization of the 10A1–2 band and adjoining region in the *Drosophila melanogaster* polytene X chromosome. Genetics **136:** 1063–1073.

Lambertsson, A., 1998 The *Minute* genes in *Drosophila* and their molecular functions. Adv. Genet. **38:** 69–134.

Liker, E., E. Fernandez, E. Izaurralde and E. Conti, 2000 The structure of the mRNA export factor TAP reveals a *cis* arrangement of a non-canonical RNP domain and an LRR domain. EMBO J. **19:** 5587–5598.

Lindsley, D. L., and G. G. Zimm, 1992 *The Genome of Drosophila melanogaster*. Academic Press, San Diego.

Mitchell, H. K., L. S. Lipps and U. M. Tracey, 1977 Transcriptional changes in pupal hypoderm in *Drosophila melanogaster*. Biochem. Genet. **15:** 575–587.

Mogami, K., and Y. Hotta, 1981 Isolation of *Drosophila* flightless mutants which affect myofibrillar proteins of insect flight muscle. Mol. Gen. Genet. **183:** 409–417.

Mogami, K., P. T. O'Donnell, S. I. Bernstein, T. R. F. Wright and C. P. Emerson, Jr., 1986 Mutations of the *Drosophila* myosin

heavy chain gene: effects on transcription, myosin accumulation and muscle function. Proc. Natl. Acad. Sci. USA **83:** 1393–1397.

Pasquinelli, A. E., R. K. Ernst, E. Lund, C. Grimm, M. L. Zapp *et al.*, 1997 The constitutive transport element (CTE) of Mason-Pfizer monkey virus (MPMV) accesses a cellular mRNA export pathway. EMBO J. **16:** 7500–7510.

Patel, N. H., B. G. Condron and K. Zinn, 1994 Pair-rule expression patterns of *even-skipped* are found in both short- and long-germ beetles. Nature **367:** 429–434.

Rosenberg-Hasson, Y., M. Renert-Pasca and T. Volk, 1996 A *Drosophila* dystrophin-related protein, MSP-300, is required for embryonic muscle morphogenesis. Mech. Dev. **65:** 83–94.

Saavedra, C., B. Felber and E. Izaurralde, 1997 The simian retrovirus-1 constitutive transport element, unlike the HIV-1 RRE, uses factors required for cellular mRNA export. Curr. Biol. **7:** 619–628.

Santos-Rosa, H., H. Moreno, G. Simos, A. Segref, B. Fahrenkrog *et al.*, 1998 Nuclear mRNA export requires complex formation between Mex67p and Mtr2p at the nuclear pores. Mol. Cell. Biol. **18:** 6826–6838.

Searles, L. L., R. S. Ruth, A.-M. Pret, R. A. Fridell and A. J. Ali, 1990 Structure and transcription of the *Drosophila melanogaster* vermilion gene and several mutant alleles. Mol. Cell. Biol. **10:** 1423–1433.

Segref, A., K. Sharma, V. Doye, A. Hellwig, J. Huber *et al.*, 1997 Mex67p, a novel factor for nuclear mRNA export, binds to both poly (A)+ RNA and nuclear pores. EMBO J. **16:** 3256–3271.

Simpson, P., R. Woehl and K. Usui, 1999 The development and evolution of bristle patterns in Diptera. Development **126:** 1349–1364.

Strässer, K., and E. Hurt, 2000 Yra1p, a conserved nuclear RNA-binding protein, interacts directly with Mex67p and is required for mRNA export. EMBO J. **19:** 410–420.

Strässer, K., J. Baßler and E. Hurt, 2000 Binding of Mex67p/Mtr2p heterodimer to FXFG, GLFG, and FG repeat nucleoporins is essential for nuclear mRNA export. J. Cell Biol. **150:** 695–706.

Stutz, F., A. Bachi, T. Doerks, I. C. Braun, B. Sèraphin *et al.*, 2000 REF, an evolutionarily conserved family of hnRNP-like proteins, interacts with TAP/Mex67p and participates in mRNA nuclear export. RNA **6:** 638–650.

Suyama, M., T. Doerks, I. C. Braun, M. Sattler, E. Izaurralde *et al.*, 2000 Prediction of structural domains of TAP reveals details of its interaction with p15 and nucleoporins. EMBO Rep. **1:** 53–58.

Tabernero, C., A. S. Zolotukhin, A Valentin, G. N. Pavlakis and B. K. Felber, 1996 The posttranscriptional control element of the Simian retrovirus type 1 forms an extensive RNA secondary structure necessary for its function. J. Virol. **70:** 5998–6011.

Tan, W., A. S. Zolotukhin, J. Bear, D. J. Patenaude and B. K. Felber, 2000 The mRNA export in *Caenorhabditis elegans* is mediated by Ce-NXF-1, an ortholog of human TAP/NXF and *Saccharomyces cerevisiae* Mex67p. RNA **6:** 1762–1772.

Tilney, L. G., P. Connelly, S. Smith and G. M. Guild, 1996 F-actin bundles in *Drosophila* bristles are assembled from modules composed of short actin filaments. J. Cell Biol. **135:** 1291–1308.

Tilney, L. G., P. S. Connelly, K. A. Vranich, M. K. Shaw and G. M. Guild, 2000 Regulation of actin filament cross-linking and bundle shape in *Drosophila* bristles. J. Cell Biol. **148:** 87–99.

Van der Bliek, A. M., and E. M. Meyerowitz, 1991 Dynamin-like protein encoded by the *Drosophila shibire* gene associated with vesicular traffic. Nature **351:** 411–414.

Van Vactor, D., and C. Kopczynski, 1999 Anatomical techniques for analysis of nervous system development in the *Drosophila* embryo, pp. 490–513 in *A Comparative Methods Approach to the Study of Oocytes and Embryos*, edited by J. Richter. Oxford University Press, New York.

Van Vactor, D., H. Sink, D. Fambrough, R. Tsoo and C. S. Goodman, 1993 Genes that control neuromuscular specificity in *Drosophila*. Cell **73:** 1137–1153.

Volk, T., and T. Yarnitzky, 1995 Laminin is required for heart, somatic muscles, and gut development in the *Drosophila* embryo. Dev. Biol. **169:** 609–618.

Zhang, H. L., R. H. Singer and G. J. Bassell, 1999 Neurotrophin regulation of β-actin mRNA and protein localization within growth cones. J. Cell Biol. **147:** 59–70.

Zhimulev, I. F., V. F. Semeshin and E. S. Belyaeva, 1981a Fine cytogenetical analysis of the band 10A1–2 and the adjoining regions in the *Drosophila melanogaster* X Chromosome. I. Cytology of the region and mapping of chromosome rearrangements. Chromosoma **82:** 9–23.

Zhimulev, I. F., A. V. Pokholkova, V. F. Bgatov, V. F. Semeshin and E. S. Belyaeva, 1981b Fine cytogenetical analysis of the band 10A1–2 and the adjoining regions in the *Drosophila melanogaster* X Chromosome. II. Genetical analysis. Chromosoma **82:** 25–40.

Communicating editor: A. J. Lopez